Radioluminescence properties under X-ray excitation of type III Ce^{3+}- and Pr^{3+}-doped $KGd(PO_3)_4$ single crystals

Irina Adell, Maria Cinta Pujol,* Rosa Maria Solé,* Magdalena Aguiló, Francesc Díaz

Universitat Rovira i Virgili, Departament Química Física i Inorgànica, Física i Cristal·lografia de Materials i Nanomaterials (FiCMA-FiCNA) - EMaS, Campus Sescelades, c/Marcel·lí Domingo, 1, E-43007 Tarragona, Spain

Abstract: The research for new scintillator materials with improved properties is gaining growing interest due to their wide variety of applications, including medical diagnosis. Here, radioluminescence studies under synchrotron X-ray excitation of bulk single crystals of type III Ce:$KGd(PO_3)_4$ and Pr:$KGd(PO_3)_4$ (Ce:KGdP and Pr:KGdP) with high crystalline quality have been carried out. The X-ray excited radioluminescence spectra show emission bands corresponding to $5d_1 \rightarrow 4f$ electronic transitions of Ce^{3+} and of Pr^{3+} in type III KGdP, being of great interest for scintillation applications. In the case of Ce:KGdP crystals, the absence of the $^6P_J \rightarrow {}^8S_{7/2}$ transitions of Gd^{3+} (~312 nm) can be ascribed to an efficient energy transfer from Gd^{3+} to Ce^{3+}. In undoped and Pr^{3+}-doped KGdP crystals, a change in coloration in the irradiated regions was observed after prolonged X-ray irradiation, which could be related to the presence of color centers

Keywords: Rare earth compound; Crystal growth; Optical spectroscopy; Radioluminescence; Synchrotron radiation; Radiation damage.

1. INTRODUCTION

Lanthanide-doped crystals, especially doped with Ce^{3+} and Pr^{3+} ions, are interesting materials for extrinsic luminescence scintillator materials. Already commercial cerium and praseodymium-doped crystals are applied as basis for many radiation detection systems. The scintillation properties required for the detectors depend on the specific application [1]. Bulk inorganic scintillators are a key component of nuclear imaging detectors [2], surgical gamma probes [3], X-ray imaging arrays [4], among others. The operation of a scintillator detector is characterized by the conversion of incident high-energy photons into flashes of ultraviolet-visible light by the action of a solid inorganic scintillator material. The scintillation light, which is desirable to be proportional to the absorbed photon energy, is converted to an electrical output signal by UV-visible detectors as silicon photomultipliers [1]. Typical inorganic scintillators which could be used are: Tl:NaI, Tl:CsI, $Bi_4Ge_3O_{12}$ (BGO), lutetium and gadolinium oxyorthosilicates Lu_2SiO_5 and Gd_2SiO_5 (LSO, GSO), cadmium tungstate $CdWO_4$ (CWO), yttrium and lutetium aluminium perovskite Ce:YAP and Ce:LuAP, and cerium-doped $LaCl_3$ and $LaBr_3$. Already commercial cerium and praseodymium-doped dielectric crystals can be potentially applied for many radiation devices. However, several shortcomings in these crystals could be improved and for this reason the search for cerium and praseodymium doped novel wide band gap materials is still currently done. Ce:LSO presents strong afterglow, high inhomogeneity of the Ce distribution along the ingots obtained by the Czochralski method, and intrinsic background signal due to the existence of the radioactive isotope ^{176}Lu [5]. Regarding Ce:GSO, one of its shortcomings is the difficulty in producing large GSO crystals because of easy cleavage [5]. Two common drawbacks in Ce:$LaCl_3$ and Ce:$LaBr_3$ are the high hygroscopicity, so they must be sealed in appropriate containers for handling and characterization [6], and the intrinsic radioactivity due to the existence of the lanthanum radio-isotope ^{138}La because it can interfere with the detection process [7]. In addition, the scintillation

*Corresponding authors.
E-mail addresses: mariacinta.pujol@urv.cat (M. C. Pujol); rosam.sole@urv.cat (R. M. Solé).

decay of Ce:$LaCl_3$ consists not only of a fast component but also a slow component on a microsecond timescale [8]. Some compounds belonging to the family of Pr-doped rare-earth halides have been studied [9,10], and none of these compounds shows a fast scintillation response, since the 5*d* level of Pr^{3+} is not populated or is non-radiatively depopulated in the scintillation mechanism.

The interest of scintillator lanthanide-doped crystals is focused on those emissions that correspond to $5d \rightarrow 4f$ transitions, and not the $4f \rightarrow 4f$ transitions. In the $5d \rightarrow 4f$ transitions of Ce^{3+}, there is a fast luminescence decay time in the order of a few nanoseconds [11]. Also, there is interest in scintillator applications for the Pr^{3+} transitions from its $5d_1$ level because it has even a shorter lifetime than Ce^{3+}, as for example of about 6 ns in the crystal of the present study, the type III $KGd(PO_3)_4$ [12].

Among the oxide crystalline scintillator materials that are being investigated recently, the polyphosphates are interesting due to their large optical transparency window, the relatively large Ln^{3+}-Ln^{3+} distance allowing high doping levels with reduced concentration quenching effect, and the possibility of being prepared in both bulk single crystal and micro and nanopowder. As pointed out by Shalapska *et al.* [13], Gd stoichiometric scintillator materials when doped with Ce^{3+} are promising due to the existence of the possibility of energy transfer from the Gd^{3+} ions constituting the host to the Ce^{3+} doping ions. Previous results about the potential of Ce-doped condensed phosphates as scintillator materials are found in the same paper of Shalapska *et al.* studying the compounds $LiREP_4O_{12}$ (RE = Gd and Y) and $NaGdP_4O_{12}$, and Zhong *et al.* for $NaGd(PO_3)_4$ [14]. Fewer reports can be found in these hosts when they are doped with Pr^{3+} [15–17].

In this work, we report on the study of X-ray excited radioluminescence of single-doped Ce:$KGd(PO_3)_4$ (hereafter Ce:KGdP) and Pr:$KGd(PO_3)_4$ (hereafter Pr:KGdP) bulk single crystals with the non-centrosymmetric (type III phase) crystalline structure. The density of type III KGdP is 3.538 $g \cdot cm^{-3}$ [18], and its effective atomic number is $Z_{eff} = 47.7$. The present spectroscopic study will contribute to the knowledge of the potential of this family of polyphosphate crystals for scintillator applications. The crystal growth technique applied leads to centimeter crystals whose size can be compatible with mid and small sized scintillators detectors.

2. EXPERIMENTAL SECTION

2.1. Bulk single crystal growth

Ce:KGdP and Pr:KGdP single crystals with type III non-centrosymmetric crystalline structure (space group: $P2_1$) and doping levels up to 1 at. % in the case of Ce^{3+} and 5 at. % in the case of Pr^{3+} substituting Gd^{3+} in the solution have been grown from high temperature solutions by the Top Seeded Solution Growth-Slow Cooling (TSSG-SC) technique. Undoped type III KGdP single crystals have also been grown by the same crystal growth technique.

The initial reagents used were K_2CO_3 anhydrous (Alfa Aesar, 99%), Gd_2O_3 (Aldrich, 99.9%), $Ce_2(CO_3)_3$ (Aldrich, 99.9%), Pr_2O_3 (Alfa Aesar, 99.9 %) and $NH_4H_2PO_4$ (Fluka Analytical, ≥99.0%). The solution compositions were 36 mol % of K_2O, 4 mol % of the sum of Gd_2O_3 plus the doping element (Ce_2O_3 or Pr_2O_3) and 60 mol % of P_2O_5. These compositions were chosen taking into account the primary crystallization region of KGdP in the K_2O–Gd_2O_3–P_2O_5 system [19]. The weight of the solutions was around 100 g for Ce:KGdP and 130 g for Pr:KGdP and KGdP, and they were prepared in platinum cylindrical crucibles of 40 and 50 mm in diameter, respectively. The high level of dynamic viscosity of the solutions (around 19 Pa·s) [20] makes difficult the solution mixing and homogenization. Thus, to improve the mixing of the solution, high thermal gradients were used, around 1.1-3.0 $K \cdot mm^{-1}$ in depth with the coolest point at the central part of the surface of the solution. Simultaneously, a Pt stirrer (18-20 mm in diameter), immersed 12-14 mm in the solution and rotating with a common axis and the same angular velocity than the crystal, was used. The crystal seed was located at 10-12 mm from the center of the solution. The seeds were cut with a^* orientation from KGdP single crystals and

were placed in contact with the solution surface with the *b* crystallographic direction tangent to the rotation movement and *c** in radial direction. The stirrer-crystal system rotated at 55 rpm with changing the rotation direction every 50 s.

After homogenizing the solution, its saturation temperature was accurately measured by studying the growth/dissolution rates at different temperatures near the saturation one. After that, starting from this temperature, the solution was slowly cooled at rates of 0.05-0.1 $K \cdot h^{-1}$ for 25-30 K to grow the crystal. Finally, the grown crystal was slowly pulled out from the liquid and cooled to room temperature at a rate of 20-25 $K \cdot h^{-1}$.

The Ce and Pr content of the crystals was determined by Electron Probe Microanalysis (EPMA) with Wavelength Dispersive Spectroscopy (WDS) using a JEOL JXA-8230. In these measurements, the accelerating voltage was 20 kV and the current 20 nA. Table 1 shows the measurement conditions used in EPMA-WDS. Using these conditions, the detection limit of Ce was 195 ppm and that of Pr was 105 ppm.

Table 1. Measurement conditions used in EPMA-WDS analysis.

Element	Standard	X-ray line	Dispersive crystal[a]	Measuring time peak / background [s]
K	KGdP	Kα	PETJ / PETJ	10 / 5
Gd	KGdP	Lα	LIFH / LIFL	10 / 5
P	KGdP	Kα	PETL / PETH	10 / 5
O	KGdP	Kα	LDE1 / LDE1	10 / 5
Ce	CeO_2	Lα	PETL / -	120 / 60
Pr	REE-1	Lα	- / LIFL	100 / 50

[a]On the left, the dispersive crystals used to measure the Ce:KGdP samples, and on the right, those used for the Pr:KGdP samples.

The distribution coefficient of Ce^{3+} and Pr^{3+} substituting Gd^{3+} in KGdP was obtained from the EPMA results and applying the formula: $K_{Ln}=([Ln]/([Ln]+[Gd]))_{crystal}/([Ln]/([Ln]+[Gd]))_{solution}$, where Ln=$Ce^{3+}$ or Pr^{3+}, and [ ] means the concentration of the element in atomic per cent.

2.2. Optical characterization

2.2.1. X-ray excited radioluminescence (RL)

The samples for optical characterization were obtained by cutting and polishing slices from the bulk single crystals obtained in this work. The slices were cut perpendicular to the *c** crystallographic direction. Ce:KGdP and Pr:KGdP with different doping levels as well as undoped KGdP single crystals were excited under several X-ray energies provided by BL22-CLAESS beamline of ALBA Synchrotron. The synchrotron radiation reached to the sample with a 45º incident angle and the radiation emitted by the sample was collected at 90º from the excitation radiation. The emitted radiation was focused using an UV fused silica biconvex lens, guided with an optical fiber and detected by an Ocean Optics FLAME-S-UV-VIS-ES spectrometer with a spectral resolution of ~1.5 nm. The emission was recorded in the range from 180 to 870 nm.

The range of energies available at BL22-CLAESS beamline of ALBA Synchrotron is from 2400 to 63000 eV. Up to 18 different excitation energies were chosen to observe whether there are differences among the RL spectra. These excitation energies are 10000, 11000, 12000, 13000, 15200, 16500, 20000, 24800, 26700, 31000, 34500, 35500, 40443, 41991, 46000, 50239, 56000 and 62500 eV. The values 40443, 41991 and 50239 eV correspond to the electron binding energies of the K label (orbital: 1s) of cerium, praseodymium and gadolinium, respectively [21]. The value 26700 eV corresponds to the band belonging to the X-ray

continuum radiation (Bremsstrahlung) from a Cu source operating at 39 kV [22]. The energy value of 24800 eV corresponds to the band belonging to the X-ray continuum radiation emitted by a Mo anode of an X-ray tube operating at 35 kV [23]. The other excitation energies have been chosen to cover the whole range of energies available and thus obtain a more complete study. The emission intensities of the RL spectra have been corrected by dividing them by the number of photons coming from the synchrotron radiation per second, which depend on the excitation energy.

2.2.2. Optical absorption

The optical absorption at room temperature was studied before and after exciting the samples by X-ray radiation in order to study the possible effects of X-rays on the samples. The measurements were carried out in the range from 190 to 800 nm. The equipment used was an Agilent Cary 5000 UV-Vis-NIR spectrophotometer.

3. RESULTS AND DISCUSSION

3.1. Bulk single crystal growth

The Ce:KGdP and Pr:KGdP single crystals obtained, with doping levels up to 1 at. % of Ce^{3+} and 5 at. % of Pr^{3+} substituting Gd^{3+} in the KGdP host, generally were transparent and without inclusions or other macroscopic defects. The dimensions of the Ce:KGdP crystals along $a^* \times b \times c^*$ directions were 3.1-6.1 mm × 9.9-15.7 mm × 9.9-13.3 mm, their weights ranged from 0.62 to 1.76 g and the crystal growth rates were generally higher than 3×10^{-3} g·h^{-1}. The sizes of the Pr:KGdP crystals along $a^* \times b \times c^*$ directions were 7.6-13.6 mm × 17.1-24.1 mm × 10.7-13.6 mm, their weights ranged from 2.73 to 6.88 g and the crystal growth rates varied from 6.1×10^{-3} to 17.4×10^{-3} g·h^{-1}. The details of these crystal growth experiments as well as the comments on the results obtained can be read in refs. [12,24]. Fig 1.a shows a photograph of an as-grown Ce:KGdP single crystal with the platinum stirrer, while Fig. 1.b shows a photograph of an as-grown Pr:KGdP single crystal with a centimeter scale.

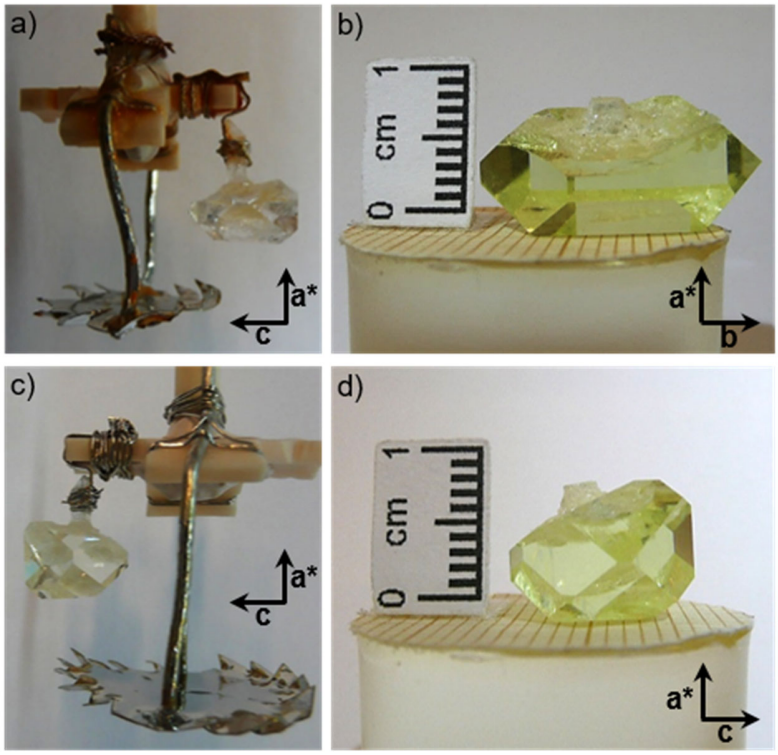

Fig. 1. a) As-grown single crystal of Ce:KGdP and platinum stirrer, b) and d) as-grown 1 at. % Pr:KGdP single crystals with the centimeter scale, and c) as-grown 0.25 at. % Pr:KGdP single crystal and platinum stirrer.

Table 2 shows the stoichiometry of the single crystals grown that have been used in the radioluminescence study. The distribution coefficients of Ce^{3+} (K_{Ce}) in KGdP calculated from the EPMA results of all the concentrations studied are higher than unity. The K_{Ce} is in the range 1.3-1.9, which means that as the crystal is growing, the concentration ratio of $Ce^{3+}/(Ce^{3+} + Gd^{3+})$ in the solution decreases [19]. In the case of Pr^{3+}-doped KGdP crystals, the distribution coefficients of Pr^{3+} (K_{Pr}) are not far from the unit [12]. In neither of the two cases, there is a significant tendency of the distribution coefficient (K_{Ce} and K_{Pr}) to decrease or increase as the level of doping in the solution increases.

Table 2. Chemical formula of the single crystals grown used in the radioluminescence measurements.

Doping element (Ln^{3+})	Atomic % of Ln^{3+} substituting Gd^{3+} in solution	Chemical formula
Ce^{3+}	0.25	$KGd_{0.996}Ce_{0.004}(PO_3)_4$
Ce^{3+}	0.50	$KGd_{0.994}Ce_{0.006}(PO_3)_4$
Ce^{3+}	1.00	$KGd_{0.981}Ce_{0.019}(PO_3)_4$
Pr^{3+}	0.25	$KGd_{0.997}Pr_{0.003}(PO_3)_4$
Pr^{3+}	1.00	$KGd_{0.990}Pr_{0.010}(PO_3)_4$
Pr^{3+}	5.00	$KGd_{0.942}Pr_{0.058}(PO_3)_4$

3.2. X-ray excited radioluminescence (RL)

3.2.1. Ce^{3+}:$KGd(PO_3)_4$ single crystals: Emission labelling

Fig. 2 shows the X-ray excited radioluminescence (RL) spectra of undoped and Ce^{3+}-doped KGdP with different doping concentrations under 16500, 24800, 35500 and 40443 eV excitation. The RL spectra of Ce:KGdP have been compared with the RL of undoped KGdP under the same excitation energies to properly label the observed emission bands. All the emission bands have been labelled by using the Dieke's diagram [25], the extended Dieke's diagram [26] and the refs. [24,27,28].

The emission bands in the RL spectra of the undoped KGdP sample (Fig. 2.a-d) belong to $4f \rightarrow 4f$ electronic transitions of Gd^{3+}. The band centered at around 312 nm corresponds to the $^6P_{3/2,\ 5/2,\ 7/2} \rightarrow {}^8S_{7/2}$ transitions. It can also be seen a band that extends from 615 to 690 nm, corresponding to the $^6G_{7/2}{}^* \rightarrow {}^6I_{11/2,\ 15/2,\ 13/2}$ and $^6G_{13/2} \rightarrow {}^6I_{7/2,\ 9/2,\ 17/2}$ transitions. In Fig. 2.a-b, some weak emission bands can be observed in the visible region that also belong to $4f \rightarrow 4f$ electronic transitions of Gd^{3+}, as shown the inset. The bands with their maximum intensity value centered at 380 and 547 nm correspond to the $^6H_{15/2} \rightarrow {}^6P_{7/2,\ 5/2}$ and $^6G_{3/2} \rightarrow {}^6P_{7/2}$ transitions, respectively. The band that starts at 400 nm and ends at 460 nm corresponds to the $^4H(2)_{7/2} \rightarrow {}^6P_{7/2}$ and $^6H_{13/2} \rightarrow {}^6I_J$ transitions, and finally, the band extending from 565 to 615 nm corresponds to the $^6G_{11/2,\ 9/2,\ 5/2} \rightarrow {}^6P_{7/2,\ 5/2}$ and $^6G_{7/2} \rightarrow {}^6P_{7/2}$ transitions. As can be observed in Fig. 2, the undoped KGdP sample emits in the visible range mainly through the $^6P_{3/2,\ 5/2,\ 7/2} \rightarrow {}^8S_{7/2}$ transitions of Gd^{3+} after being excited under X-ray radiation.

In the RL spectra of the Ce^{3+}-doped type III KGdP samples (space group: $P2_1$), it can be observed an intense band that extends from 300 to 385 nm and that is formed by the overlapping of two bands corresponding to the $5d_1 \rightarrow {}^2F_{5/2}$ and $5d_1 \rightarrow {}^2F_{7/2}$ transitions of Ce^{3+} in KGdP, respectively. These two electronic transitions were already observed in a previous work [24] as a doublet band centered at 322 and 342 nm in the emission spectra of the same samples under VUV-UV excitation (direct $4f \rightarrow 5d$ excitation), confirming that these emissions of the RL spectra are originated from the active Ce^{3+} ions. This band is presented as a doublet because the $^2F_{5/2}$ and $^2F_{7/2}$ levels are separated by 2000 cm^{-1} [25]. In radioluminescence studies of compounds of the same family performed by Zhong *et al.* on Ce^{3+}-doped $MGdP_4O_{12}$ (M = Li, Na, K, Cs) under X-ray irradiation [14], the doublet band corresponding to the $5d_1 \rightarrow {}^2F_{5/2}$ and $5d_1 \rightarrow {}^2F_{7/2}$ transitions of Ce^{3+} has been observed centered at 310 and 329 nm for $Ce:LiGdP_4O_{12}$ (space group: $C2/c$), 314 and 333 nm for $Ce:NaGdP_4O_{12}$ (space group: $P2_1/n$), 325 and 345 nm for $Ce:KGdP_4O_{12}$ (space group: $C2/c$, type B phase), 336 and 358 nm for $Ce:CsGdP_4O_{12}$ (space group: $P2_1/n$). As observed in the RL results of the two crystalline phases of $KGd(PO_3)_4$ mentioned (type III, studied in our work, and type B, in the ref. [14]), its polymorphism does not significantly affect the energy values of these $4f$ and $5d$ levels of Ce^{3+}.

Simultaneously, other bands with a lower intensity can also be observed in the visible region from 375 to 700 nm, and correspond to the $4f \rightarrow 4f$ transitions of Gd^{3+} mentioned in the RL spectra of the undoped KGdP samples.

It is interesting to note that the band corresponding to the $^6P_{3/2,5/2,7/2} \rightarrow {}^8S_{7/2}$ transitions of Gd^{3+} (around 312 nm) is not observed when Ce^{3+} is present in the crystal, even at low Ce^{3+} concentrations (0.25 at. %).

The radioluminescence under X-ray excitation has been studied for different doping levels to observe the effect of the Ce^{3+} concentration. In Fig. 2, it can be seen that the intensity of the band corresponding to the $5d_1 \rightarrow {}^2F_{5/2}$ and $5d_1 \rightarrow {}^2F_{7/2}$ transitions of Ce^{3+} varies depending on the Ce^{3+} concentration, while the most intense Gd^{3+} band around 660 nm is maintained around the same intensity value at a specific excitation energy, whatever the doping level of Ce^{3+}. The decrease of the Ce^{3+} emission in the case of 1 at. % Ce:KGdP crystal with respect to the crystal of 0.5 at. % Ce:KGdP could be due to the reabsorption of the emission of a Ce^{3+} ion by its neighboring Ce^{3+} ions.

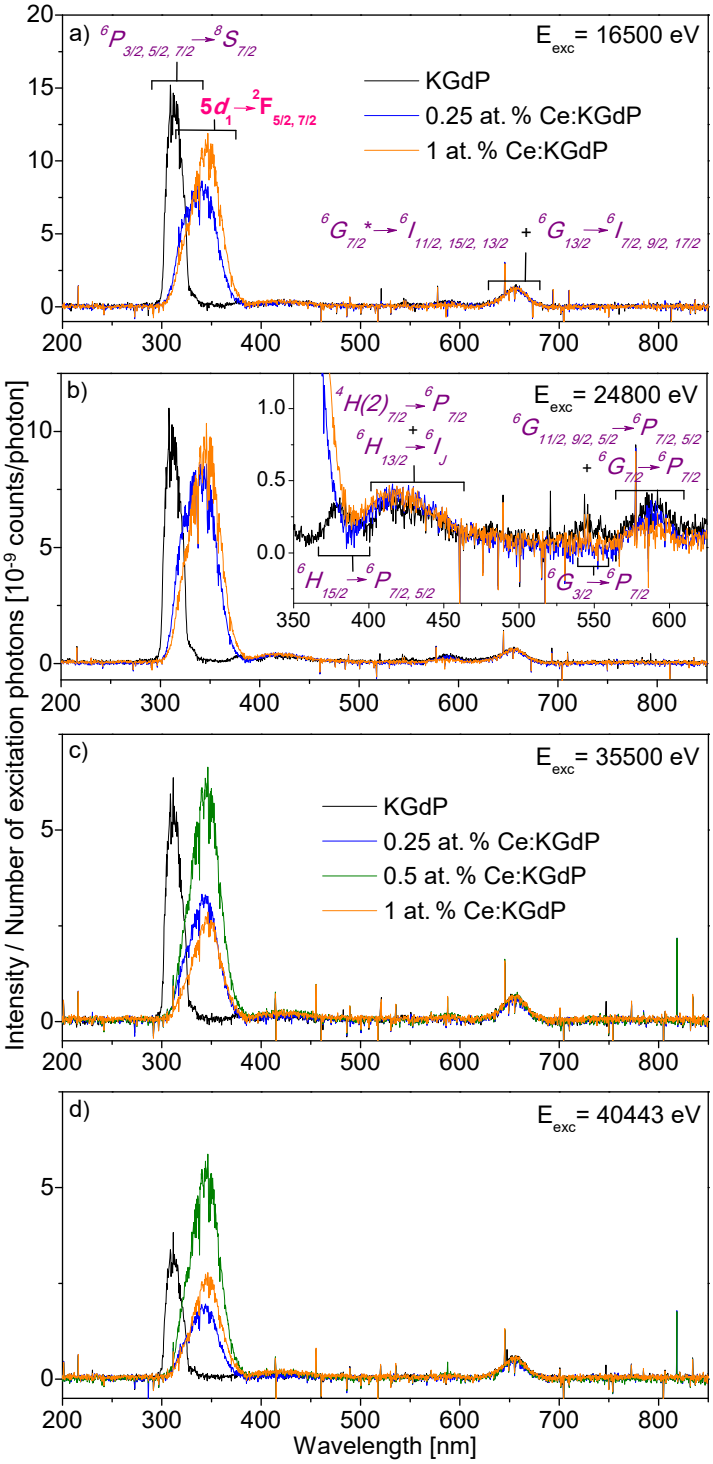

Fig. 2. X-ray excited radioluminescence spectra of KGdP and Ce:KGdP at different Ce^{3+} concentrations under excitation at a) 16500 eV, b) 24800 eV, c) 35500 eV and d) 40443 eV. Labels in purple and italics indicate the electronic transitions of Gd^{3+} and labels in pink and bold those of Ce^{3+}.

3.2.2. Ce^{3+}:$KGd(PO_3)_4$ single crystals: Proposed mechanism

In cerium-doped scintillation materials, most of the energy absorbed by the material after its excitation with X-ray radiation is used for the formation of electron−hole pairs [29]. Consequently, in such materials, most of the localized excitations are electron−hole pairs and, therefore, the energy transfer process to Ce^{3+} ions is based on the sequential capture of charge carriers by Ce centers [29−33]. Since Ce^{3+} is a good hole trap [32,34,35], in Ce^{3+}-doped crystals, the energy transfer process usually begins with the capture of a hole by Ce^{3+} and then of an electron by Ce^{4+}. The hole trap cross section of Ce^{3+} strongly depends on the energy difference between the 4*f* ground state of Ce^{3+} in the forbidden bandgap and the top of the valence band of the crystal, i.e. the lower the energy difference, the higher the efficiency of the capture of a hole by Ce^{3+} [29,31,32,35−37]. A high scintillation efficiency is connected with a high probability of hole capture [29,36]. It is worth mentioning that the initial coexistence of Ce^{4+} and Ce^{3+} ions in the scintillation crystal sometimes can be harmful because Ce^{4+} is an efficient electron trap and, therefore, can compete with Ce^{3+} for the capture of charge carriers and induce severe limitations in scintillation efficiency [31,34]. However, recent research has shown that the presence of a stable Ce^{4+} center is not always harmful, but can positively influence [38,39,40], so their relative ratio must be adequately tuned for material optimization [41].

So given the above information, after exciting the type III Ce:KGdP single crystals with X-ray radiation, most of the electronic excitations created in the crystal are electron−hole pairs and the energy transfer process to the Ce^{3+} ions is through a sequential capture of charge carriers. In these crystals, the presence of Ce^{4+} is not expected because this ion is not present in the initial reagents and because the crystalline network resulting from the partial substitution of Gd^{3+} by Ce^{3+} is electrically neutral, with a higher stability than the resulting from the partial substitution by Ce^{4+}. Therefore, there would be no competition between the Ce^{4+} and Ce^{3+} ions in Ce:KGdP. In addition to this, it is interesting to mention that Gd^{3+} ion is very unlikely to introduce both hole and electron traps in materials and, for this reason, it is one of the two best candidates (together with Lu) to act as a neutral constituent in scintillation materials [32]. Thus, the energy transfer from the correlated electron−hole pairs to the emitting centers is expected to be more effective for Ce^{3+} ions than for Gd^{3+} ions, although it should be noted that the concentration of Gd^{3+} is considerably higher than that of Ce^{3+}. Once the emitting centers are excited, radioluminescence can be produced by these centers. Probably because of the above-mentioned facts, the emission band corresponding to the $5d_1 \rightarrow {}^2F_J$ transitions of Ce^{3+} is very intense, and simultaneously, weak emission bands corresponding to some transitions between the 4*f* high energy levels of Gd^{3+} can be observed.

The localization of the 5*d* and 4*f* levels of Ce^{3+} and Gd^{3+} with respect to conduction and valence bands in type III KGdP is shown in Fig. 3.a. The energy difference between the $5d_1$ level of Ce^{3+} in KGdP and the bottom of the conduction band is expected to be similar to the one of Ce^{3+} doped $LiYP_4O_{12}$, determined in the work of Dorenbos *et al.* [42], due to the high similarity with our host. The other 5*d* levels and all 4*f* levels of Ce^{3+} have been located with respect to the $5d_1$ level of Ce^{3+} in KGdP taking into account the spectroscopic studies performed in our previous work [24]. Since the energy difference between the $5d_1$ level of Ce^{3+} and that of Gd^{3+} is maintained independently of the host [42], the $5d_1$ level of Gd^{3+} in KGdP has also been located with respect to the conduction and valence bands. The 4*f* levels of Gd^{3+} have been located with respect to its $5d_1$ level in KGdP taking into account the spectroscopic studies performed in our previous work [12], the extended Dieke's diagram [26] and the refs. [27,28].

Below, several works related to radioluminescence studies of Gd^{3+}-containing hosts doped with Ce^{3+} are summarized, focusing on the Ce^{3+} emissions corresponding to the $5d_1 \rightarrow {}^2F_J$ transitions, the Gd^{3+} emission at 312 nm and the possible energy transfer between Ce^{3+} and Gd^{3+} ions [14,43−45].

In the work done by Zhong *et al.* previously mentioned about the radioluminescence properties of Ce^{3+}-doped $MGdP_4O_{12}$ (M = Li, Na, K, Cs) [14], it can be seen that the peak of

Gd^{3+} at 312 nm clearly stands out from the band corresponding to the $5d_1 \rightarrow {}^2F_{5/2}$ transition of Ce^{3+} for Ce:$LiGdP_4O_{12}$, while it becomes weaker for Ce:$NaGdP_4O_{12}$. By contrast, the peak disappears completely for Ce:$KGdP_4O_{12}$ and Ce:$CsGdP_4O_{12}$. Therefore, as mentioned in their work, the energy transfer from Gd^{3+} to Ce^{3+} becomes more efficient as the M^+ radius increases.

The condition for Gd → Ce energy transfer from the ${}^6P_J$ levels of Gd^{3+} to the $5d_1$ level of Ce^{3+} is satisfied when there is no energy difference between the energy levels of ${}^6P_J$ and the absorption edge of the $4f \rightarrow 5d$ transitions of Ce^{3+}. The efficiency of this energy transfer becomes higher as the degree of overlap between the ${}^6P_J$ levels of Gd^{3+} and the Ce^{3+} absorption spectrum increases. These affirmations were confirmed in the work done by Shalapska *et al.* on the luminescence properties of $LiGd_{0.9}Ce_{0.1}P_4O_{12}$, $LiY_{0.9}Ce_{0.1}P_4O_{12}$ (both, space group: $C2/c$) and $NaGd_{0.9}Ce_{0.1}P_4O_{12}$ (space group: $P2_1/n$) upon vacuum-ultraviolet and X-ray excitation [46]. The doublet band corresponding to the $5d_1 \rightarrow {}^2F_{5/2}$ and $5d_1 \rightarrow {}^2F_{7/2}$ transitions of Ce^{3+} is observed in the X-ray excited emission spectra of the three compounds, while the peak of Gd^{3+} at 312 nm is present in the spectra of the two Gd^{3+}-containing phosphates.

In the research carried out by Liang *et al.* into the photoluminescence and radioluminescence of undoped and Ce^{3+}-activated $Na_3Gd(PO_4)_2$ [43], the X-ray excited radioluminescence spectrum of $Na_3Gd_{0.99}Ce_{0.01}(PO_4)_2$ shows an intense band that is formed by the overlapping of two bands centered at 341 and 365 nm that corresponds to the $5d_1 \rightarrow {}^2F_{5/2}$ and $5d_1 \rightarrow {}^2F_{7/2}$ transitions of Ce^{3+} in this host, respectively. The peak centered at 312 nm corresponding to the ${}^6P_J \rightarrow {}^8S_{7/2}$ transitions of Gd^{3+} is not present in the spectrum mentioned above, which according to the authors implies that the energy transfer from the ${}^6P_J$ states to Ce^{3+} is efficient.

The X-ray excited radioluminescence of Ce^{3+}-doped multicomponent garnets with formula unit $(Ce_xGd_yR_{1-x-y})_3(Ga_zAl_{1-z})_5O_{12}$ (R = Y or Lu) have been studied by Kucera *et al.* at different Gd^{3+} doping concentrations [44]. In all Gd^{3+} concentrations studied, the emission band corresponding to the $5d_1 \rightarrow {}^2F_{5/2,7/2}$ transitions of Ce^{3+} is shown as a single broad band centered at approximately 510 nm. The authors concluded that for Gd^{3+} concentrations below 5 at. %, the total emission of the sample originates from two emission centers, Ce^{3+} and Gd^{3+}, with the $5d_1 \rightarrow {}^2F_J$ emission of Ce^{3+} and the ${}^6P_J \rightarrow {}^8S_{7/2}$ emission of Gd^{3+} (maximum near 312 nm). At higher Gd^{3+} concentrations (<50 at. %), the Ce^{3+} emission increases gradually while the Gd^{3+} emission decreases and the total integrated emission of the sample is significantly higher than the previous case, so that the Gd^{3+} receives the energy and contributes to increase the intensity of the Ce^{3+} emission through an energy transfer to Ce^{3+} ions. The Gd^{3+} emission peak disappears completely at Gd^{3+} concentrations ~50 at. % and higher caused by the energy migration across the Gd^{3+} ions and an efficient energy transfer from Gd^{3+} to Ce^{3+} that is favored due to the downwards shift of the $5d$ levels of Ce^{3+}, since the increase of gadolinium content in the sample increases the crystal field.

In our case, in the X-ray excited radioluminescence spectra of type III Ce:KGdP single crystals, the band corresponding to the ${}^6P_J \rightarrow {}^8S_{7/2}$ transitions of Gd^{3+} (~312 nm) is not present, so it can be attributed to a very efficient non-radiative energy transfer process from the ${}^6P_J$ levels of Gd^{3+} to the $5d_1$ level of Ce^{3+}, as happened in other Gd^{3+}-containing hosts doped with Ce^{3+} [14,43−45]. Also, a bidirectional energy transfer between the $5d_5$ level of Ce^{3+} and the ${}^6F_J$ and ${}^6G_J$ levels of Gd^{3+} might take place, which was also observed in photoluminescence studies in our previous work [24], since some emission bands corresponding to the electronic transitions from the ${}^6G_J$ levels to the ${}^6I_J$ and ${}^6P_J$ levels of Gd^{3+} have been observed. Therefore, different bidirectional energy transfer processes between Ce^{3+} and Gd^{3+} ions are expected. Although, it is clear that Gd^{3+} receives energy directly from the localized excitations because some of the Gd^{3+} emission bands that appear in the radioluminescence spectra correspond to electronic transitions starting from the ${}^6H_J$ and ${}^4H(2)_{7/2}$ levels of Gd^{3+}, which have higher energy than the $5d_5$ level of Ce^{3+} in type III KGdP. The different energy transfer processes can be observed in Fig. 3.b.

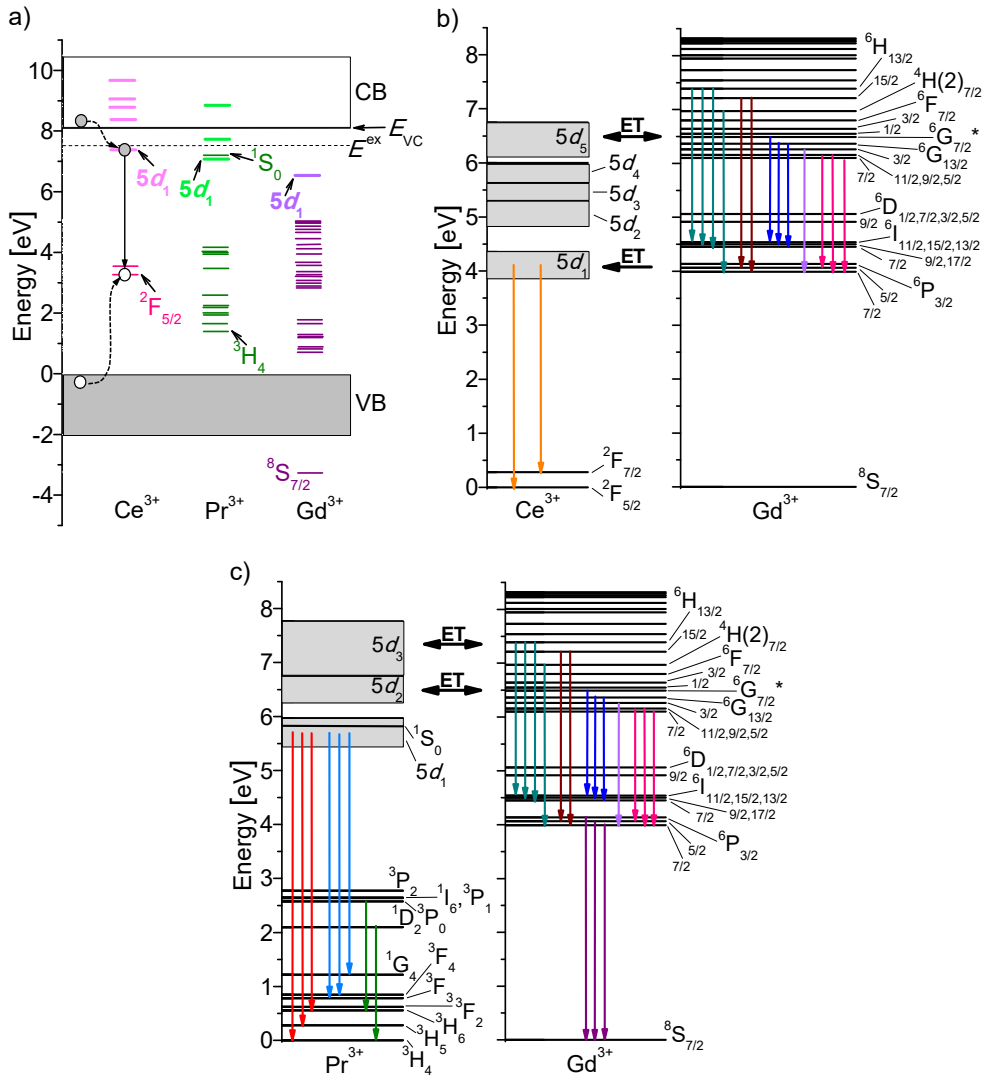

Fig. 3. a) Energy levels scheme for Ce^{3+}, Pr^{3+} and Gd^{3+} with respect to conduction (CB) and valence bands (VB) of type III $KGd(PO_3)_4$, which schematically illustrates the energy transfer process corresponding to a fast decay rate for the Ce^{3+} case [47]. The refs. [12,24,42] have been used to place the energy levels in this host. b) Energy level diagram of Ce^{3+} and Gd^{3+} in $Ce:KGd(PO_3)_4$ and emissions observed under X-ray excitation. The arrows of the same color appear as a single band in the radioluminescence spectra. c) Energy level diagram of Pr^{3+} and Gd^{3+} in $Pr:KGd(PO_3)_4$ and emissions observed under X-ray excitation.

3.2.3. Pr^{3+}:$KGd(PO_3)_4$ single crystals: Emission labelling

A similar study to that performed with the previous Ce:KGdP samples, has been carried out with Pr:KGdP single crystals. Fig. 4 shows the X-ray excited radioluminescence (RL) spectra of undoped and Pr^{3+}-doped type III KGdP (space group: $P2_1$) with different doping concentrations under 12000, 16500, 31000 and 46000 eV excitation. The emission intensities have been corrected by dividing them by the corresponding number of excitation photons per second for each excitation energy. The RL spectra of undoped KGdP have been used to correctly label the emission bands that appear in the spectra of Pr:KGdP. As mentioned in the

previous study, the assignation of each emission band has been made by taking into account the Dieke's diagram [25], the extended Dieke's diagram [26] and the refs. [12,27,48].

Unlike Ce^{3+}-doped samples, the most intense emission band in all RL spectra of undoped and Pr^{3+}-doped KGdP samples is centered at 312 nm corresponding to the $^6P_{3/2,5/2,7/2} \rightarrow {}^8S_{7/2}$ transitions of Gd^{3+}. In the RL spectra of Pr:KGdP, two bands centered around 236 and 259 nm can be observed. They belong to $5d \rightarrow 4f$ transitions of Pr^{3+} in KGdP, which correspond more specifically to the $5d_1 \rightarrow {}^3H_{4,5,6}, {}^3F_2$ and $5d_1 \rightarrow {}^3F_{3,4}, {}^1G_4$ transitions, respectively. It is reaffirmed that these two emissions are originated from the active Pr^{3+} ions, since in our previous work regarding the luminescence properties of the same samples under VUV-UV excitation (direct $4f \rightarrow 5d$ excitation) [12], these and others bands corresponding to $5d \rightarrow 4f$ transitions of Pr^{3+} were also observed, such as the emission bands centered at 229, 239, 256, 265 nm, 358 and 435 nm labelled as the $5d_1 \rightarrow {}^3H_5$, $5d_1 \rightarrow {}^3H_6, {}^3F_2$ $5d_1 \rightarrow {}^3F_{3,4}$, $5d_1 \rightarrow {}^1G_4$, $5d_1 \rightarrow {}^1D_2$ and $5d_1 \rightarrow {}^3P_2$ transitions of Pr^{3+} in KGdP, respectively.

As regards to the spectral range from 350 to 850 nm, the broad band that extends from 560 to 700 nm when the crystals are excited at 12000 eV (Fig. 4.a) could be attributed to the $^1D_2 \rightarrow {}^3H_4$ and $^3P_0 \rightarrow {}^3H_6$ transitions of Pr^{3+} since this band does not appear in the RL spectrum of undoped KGdP nor in that of the crystal with low Pr^{3+} content. This emission band has also been observed in the X-ray excited radioluminescence spectra of 0.3 at. % $Pr:(Gd,Lu)_3Ga_3Al_2O_{12}$ [49], 1 at. % $Pr:K_3(Lu,Y)(PO_4)_2$ [50], $Pr:Lu_2Si_2O_7$ [51], 0.2 at. % $Pr:Lu_3Al_5O_{12}$ [52], 0.2 and 2 at. % $Pr:Ca_3Sc_2Si_3O_{12}$ [53]. When the excitation energies are 16500 eV (Fig. 4.b), 31000 eV (Fig. 4.c) and 46000 eV (Fig. 4.d), all the emission bands that appear in the wavelength range from 360 to 725 nm belong to $4f \rightarrow 4f$ transitions of Gd^{3+} since these bands also appear in the RL spectra of undoped KGdP. The labelling of Gd^{3+} electronic transitions is the same as in the RL spectra of the Ce:KGdP samples.

The effect of the Pr^{3+} concentration has been studied for three different doping levels at several excitation energies. In the spectra obtained under 12000 eV excitation (Fig. 4.a), it can be observed that in Ce:KGdP there is an increase of the photon conversion in the range from 200 to 350 nm in comparison with the undoped crystal, that is, there is a higher intensity of the overall emission in this range when Pr^{3+} is present in the crystal. When the crystal is doped with 5 at. % Pr^{3+}, the intensity of the $5d_1 \rightarrow 4f$ bands of Pr^{3+} is even higher than that observed in the crystal with 1 at. % Pr^{3+}, so there is no concentration quenching effect by Pr^{3+} concentration up to the value studied. In addition to this, it can also be observed that the intensity of the Gd^{3+} band decreases gradually. Since the bands belonging to Pr^{3+} increase and the Gd^{3+} band decreases in intensity when the Pr^{3+} content increases, it seems that there is an increase in efficiency in the energy transfer from Gd^{3+} to Pr^{3+}. This energy transfer could be from the Gd^{3+} $4f$ levels of higher energy to the Pr^{3+} $5d_{2,3}$ levels, followed by a non-radiative relaxation to the $5d_1$ level. The different energy transfer processes are depicted in Fig. 3.c.

Under 16500 eV (Fig. 4.b) and 31000 eV (Fig. 4.c) excitations, it can be seen that the Gd^{3+} band centered at 312 nm clearly varies depending on the Pr^{3+} concentration, while the Pr^{3+} bands (236 and 259 nm) and the other Gd^{3+} bands practically remain with the same intensity value. Since the intensity of the Gd^{3+} band centered at 312 nm is higher when the doping level is 0.25 and 1 at. % of Pr^{3+} with respect to the undoped KGdP and, at the same time, the $5d_1 \rightarrow 4f$ bands of Pr^{3+} have a similar intensity in the two concentrations, this could mean that there is an energy transfer from the Pr^{3+} $5d_{2,3}$ levels to the ^6G_J levels and other $4f$ levels of higher energy of Gd^{3+}, followed by the $^6G_J \rightarrow {}^6I_J$, ^6P_J radiative transitions of Gd^{3+} and then the $^6P_J \rightarrow {}^8S_{7/2}$ more intense transitions. So, there are bidirectional energy transfer processes between Pr^{3+} doping ions and Gd^{3+} ions constitutive of the host.

When the studied crystals are excited with energies from 35500 to 62500 eV (Fig. 4.d), a clearly different behavior can be observed according to the Pr^{3+} concentration in comparison with the spectra explained above. In this energy range, the 1 at. % Pr:KGdP crystal shows a higher emission intensity than the other Pr^{3+}-doped samples.

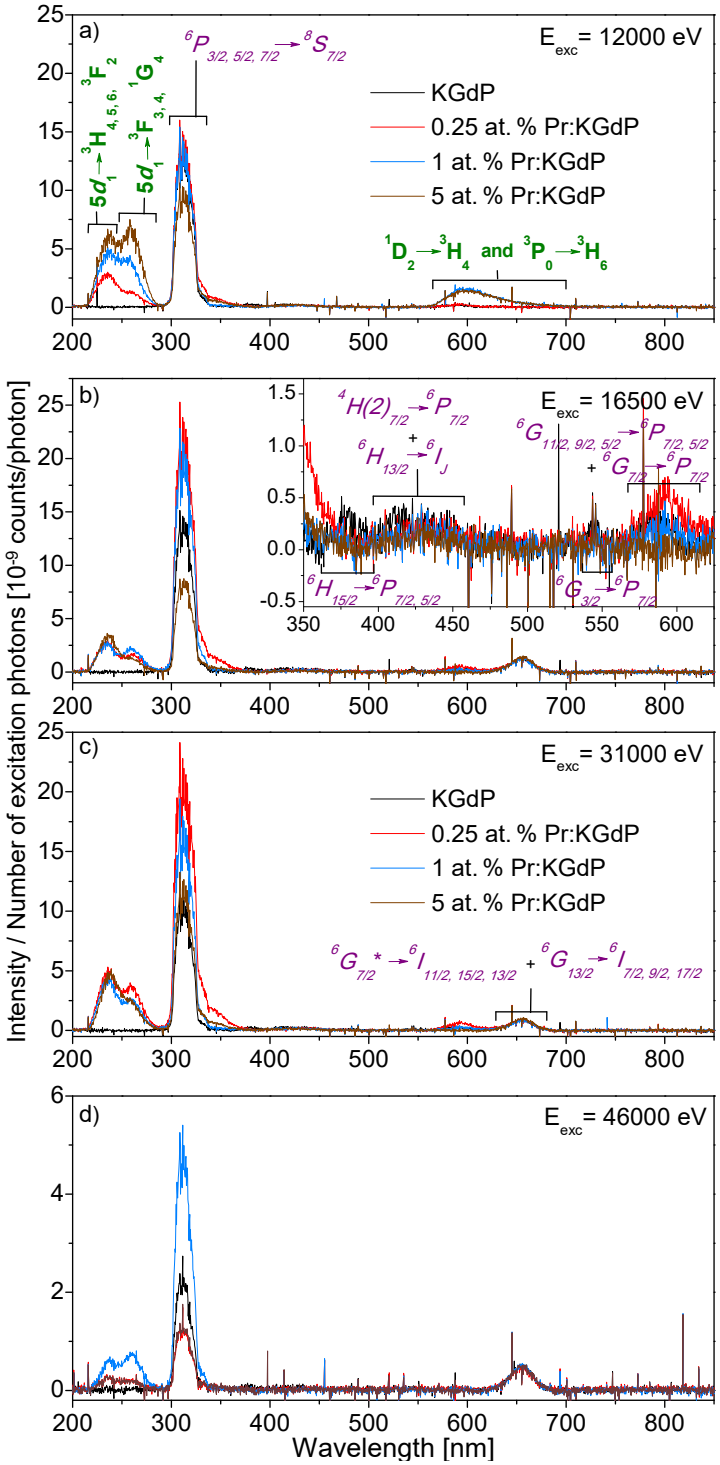

Fig. 4. X-ray excited radioluminescence spectra of KGdP and Pr:KGdP at different Pr^{3+} concentrations under excitation at a) 12000 eV, b) 16500 eV, c) 31000 eV and d) 46000 eV. Labels in purple and italics indicate the electronic transitions of Gd^{3+} and labels in green and bold those of Pr^{3+}.

3.2.4. Pr^{3+}:$KGd(PO_3)_4$ single crystals: Proposed mechanism

In praseodymium-doped scintillation materials, the energy transfer process based on the sequential capture of charge carriers by Pr centers usually begins with the capture of a hole because Pr^{3+} is a good candidate for hole trap [32,35]. Analogous to the explanation of the Ce^{3+}-doped crystals (see section 3.2.2), the efficiency of hole capture by Pr^{3+} ions strongly depends on the energy difference between the top of the valence band of the crystal and the 4*f* ground state of Pr^{3+} in the forbidden bandgap [35]. The smaller the energy difference mentioned, the higher the efficiency of hole capture, which is connected with a higher scintillation efficiency. Moreover, it is worth mentioning that in gadolinium-containing scintillation materials, Gd^{3+} ion acts as a neutral constituent because it is very unlikely to introduce both hole and electron traps [32].

Therefore, in our case, after the creation of electronic excitations in the crystal lattice of the type III Pr:$KGd(PO_3)_4$ single crystals caused by X-ray irradiation, energy transfer processes from the localized excitations to the Pr^{3+} and Gd^{3+} ions take place [30,31]. When the localized excitations are electron−hole pairs, the energy transfer process from them to the emitting centers is expected to be more effective for Pr^{3+} ions than for Gd^{3+} ions, although it has to be taken into account that the concentration of Pr^{3+} is significantly smaller than that of Gd^{3+} in Pr:$KGd(PO_3)_4$.

The 5*d* and 4*f* levels of Pr^{3+} and Gd^{3+} have been located with respect to the conduction and valence bands in type III KGdP, as shown Fig. 3.a. First, the $5d_1$ level of Ce^{3+} has been located with respect to the bottom of the conduction band of type III KGdP assuming the same energy difference observed in the energy levels scheme for polyphosphate $LiYP_4O_{12}$ in the ref. [42] due to the high similarity between these hosts. Then, since the energy difference between the $5d_1$ level of Ce^{3+} and the $5d_1$ levels of the other lanthanides (Ln^{3+}) is maintained independently of the host [42], the $5d_1$ level of Pr^{3+} and that of Gd^{3+} have been located with respect to the conduction band. Finally, the other 5*d* levels and the 4*f* levels of Pr^{3+} have been located with respect to the $5d_1$ level of Pr^{3+} taking into account the spectroscopic studies performed in our previous work [12], and the 4*f* levels of Gd^{3+} have been located with respect to its $5d_1$ level considering the mentioned work [12], the extended Dieke's diagram [26] and the refs. [27,28].

As shown in Fig. 4, once the Pr^{3+} and Gd^{3+} ions are excited, these centers emit light. Since the bands corresponding to the $5d_1 \rightarrow 4f$ transitions of Pr^{3+} and to the $^6P_J \rightarrow {}^8S_{7/2}$ transitions of Gd^{3+} are clearly present, the presence of this Gd^{3+} emission may be ascribed to an inefficient energy transfer process from the ^6D_J, ^6I_J and ^6P_J levels of Gd^{3+} to the $5d_1$ level of Pr^{3+}. This is due to the relatively high energy difference between the mentioned levels of the two ions in Pr:KGdP, and also the fact that the $5d_1$ is slightly higher in energy than the Gd^{3+} mentioned levels. The coexistence of these bands has also been observed in the X-ray excited radioluminescence spectra of some stoichiometries of the following Gd-based multicomponent aluminate garnets: 0.3 at. % Pr:$(Gd,Lu)_3Ga_3Al_2O_{12}$ [49], 0.2 and 1 at. % Pr:$(Gd,Lu)_3(Ga,Al)_5O_{12}$ [54]. In the work done by Wu and Ren [49], radioluminescence spectra of the multicomponent garnet 0.3 at. % Pr:$(Gd,Lu)_3Ga_3Al_2O_{12}$ were obtained at different Gd/Lu ratios and then compared. For $Gd_{0.025}Lu_{2.975}$, $Gd_{0.05}Lu_{2.95}$ and $Gd_{0.1}Lu_{2.9}$ samples, their spectra show the Gd^{3+} emission belonging to the $^6P_{7/2} \rightarrow {}^8S_{7/2}$ transition at about 311 nm, the Pr^{3+} bands corresponding to the $5d_1 \rightarrow {}^3H_4$, $5d_1 \rightarrow {}^3H_5$, $5d_1 \rightarrow {}^3H_6$,$^3F_2$ and $5d_1 \rightarrow {}^3F_{3,4}$ transitions around 295, 305, 320 and 330 nm, respectively, and the Pr^{3+} bands that belong to several $4f \rightarrow 4f$ transitions in the spectral range from 450 to 650 nm. Whereas the spectra of $Gd_{0.2}Lu_{2.8}$, $Gd_{0.4}Lu_{2.6}$ and $Gd_{0.6}Lu_{2.4}$ samples show that, the bands corresponding to the $5d_1 \rightarrow 4f$ transitions of Pr^{3+} become irrelevant. A reduction in the intensity of the $5d_1 \rightarrow 4f$ bands of Pr^{3+} can be observed accompanied with a significant enhancement of the Gd^{3+} emission as the Gd^{3+} content increases. The authors attribute this behavior to an energy transfer from the 5*d* levels of Pr^{3+} to the 4*f* levels of Gd^{3+}. In the second work, done by Kamada *et al.* [54], the spectrum of 0.2 at. % Pr:$Gd_{0.5}Lu_{2.5}Ga_2Al_3O_{12}$ shows, in the range from 200 to 450 nm, clearly a broad band that extends from 290 to 420 nm, which corresponds to the $5d_1 \rightarrow 4f$ transitions of Pr^{3+}, and a hump

with the maximum of intensity at 312 nm, which belongs to the $^6P_{7/2} \rightarrow {}^8S_{7/2}$ transition of Gd^{3+}. After increasing the Gd/Lu ratio to 0.5, it can be observed in the spectrum of the resulting sample that the Gd^{3+} band is narrow and intense and that the Pr^{3+} bands are practically non-existent.

In our case, the emission bands corresponding to the Pr^{3+} $5d_1 \rightarrow 4f$ transitions are present, despite the high atomic concentration of Gd^{3+} in the crystal. Besides, in contrast to the aforementioned inefficient energy transfer between the ^6D_J, ^6I_J and ^6P_J levels of Gd^{3+} and the $5d_1$ level of Pr^{3+}, bidirectional energy transfer processes between the Pr^{3+} $5d_{2,3}$ levels and the Gd^{3+} $4f$ levels of higher energy are expected (Fig. 3.c) taking into account the discussion on the effect of the Pr^{3+} concentration (section 3.2.3).

3.3. Radiation damage in $KGd(PO_3)_4$ samples

As it is known, crystalline scintillators may suffer from radiation damage under continued X-ray and γ-ray irradiation. The most common damage is the appearance of radiation-induced absorption bands, which are caused by the formation of color centers. The color centers may be electrons located in anion vacancies (F center) of the crystalline lattice, or holes located in cation vacancies (V center), or others. In oxides, the radiation damage usually consists of defects related to stoichiometry, such as oxygen vacancies. The missing of oxygen in the crystalline lattice leads to the existence of anion vacancies that act as traps for electrons. The color centers can disappear at room temperature, although the recovery speed depends on the depth of the traps [55].

During the radioluminescence measurements (section 3.2), some KGdP samples changed their color in the region where they were being excited under prolonged X-ray irradiation. A dark brownish region was observed in the undoped sample and a brown-yellowish region in the Pr-doped KGdP samples, as shown in Fig. 5. This behavior was not observed in the Ce-doped samples (Fig. 5.b). The colored regions disappeared with time (in a few hours), indicating an apparent recovery of the samples. This change in coloration has been reported for other crystals after being excited with ionizing radiation, such as $Pr:Ca_3Sc_2Si_3O_{12}$ under X-ray irradiation [53], $Gd:PbWO_4$ irradiated with neutrons [56], and $Mn:Bi_4Ge_3O_{12}$ under γ-ray irradiation [55, 57]. Regarding $Pr:Ca_3Sc_2Si_3O_{12}$, apart from the color change, the authors observed a deviation of X-ray excited decay curves from exponential behavior and faster decay components compared to those observed under VUV excitation. This behavior was assigned to the creation of radiation defects which act as quenching centers in the scintillator activity [53]. In the case of $Gd:PbWO_4$ crystals, the authors attributed the change in color from colorless to violet to the absorption of the inherent clusters of WO_{3-x} in the regular lattice of $PbWO_4$ that, after irradiation, change the valence of tungsten gradually (from W^{6+} via W^{5+} to W^{4+}) depending on the radiation dose applied, resulting in different optical absorption spectra and, consequently, different colors of the crystal [56]. For $Mn:Bi_4Ge_3O_{12}$, the authors noted that the crystal turned pinkish immediately after γ-ray irradiation and observed some radiation-induced absorption bands that extend from the absorption edge of BGO (306 nm) to approximately 750 nm and are centered at 326, 413 and 539 nm. The same radiation-induced absorption bands were found in a series of 24-doped BGO samples and in all cases, they were assigned to color centers related to defects of the crystal lattice, such as oxygen vacancies [57].

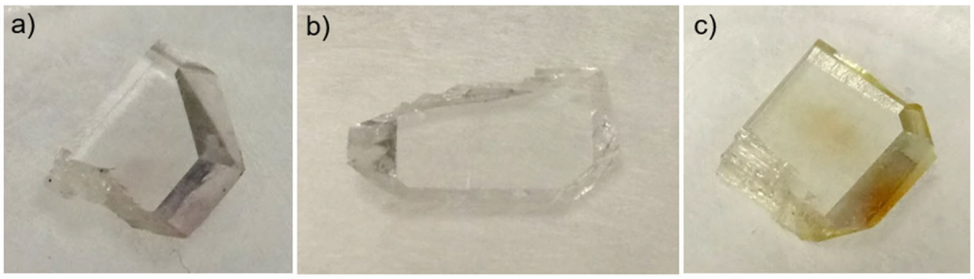

Fig. 5. a) Undoped KGdP, b) 1 at. % Ce:KGdP and c) 1 at. % Pr:KGdP single crystals just after continued X-ray irradiation.

In order to study these phenomena, the optical absorption of several KGdP samples was measured, comparing the spectrum obtained before the X-ray irradiation with that performed after several days of recovering (5-7 days). Fig. 6 shows the optical absorption spectra of the three different types of samples studied in this work, undoped, Ce-doped and Pr-doped KGdP, together with the spectra resulting from the subtraction of the first data (before irradiation) from the second one (after irradiation). The absorption peaks present in the optical absorption spectra of the undoped KGdP sample (Fig. 6.a) in the spectral range from 190 to 320 nm correspond to $4f \rightarrow 4f$ transitions of Gd^{3+}. As can be seen in the subtraction spectrum, there is an increase in absorbance from 190 to 600 nm after X-ray irradiation. In relation to the Ce-doped KGdP sample (Fig. 6.b), the broad and intense band observed in the optical absorption spectra corresponds to the $^2F_{5/2} \rightarrow 5d_x$ transitions of Ce^{3+} along with the same $4f \rightarrow 4f$ transitions of Gd^{3+} present in the undoped sample, as clearly shown in our previous work [24]. In the corresponding subtraction spectrum, it can be seen that the broad radiation-induced absorption band present in the previous sample is not present in the case of Ce-doped KGdP. About the optical absorption spectra of the Pr-doped KGdP sample (Fig. 6.c), the broad and intense band centered around 218 nm corresponds to the $^3H_4 \rightarrow 5d_1$ transition of Pr^{3+}, while the absorption peaks within the spectral range from 425 to 625 nm correspond to some $4f \rightarrow 4f$ transitions of Pr^{3+} (as shown in our previous work [12]) and the other peaks correspond to Gd^{3+} $4f \rightarrow 4f$ transitions. In the subtraction spectrum, it can be seen an increase in absorbance from 190 to 600 nm after X-ray irradiation with a maximum intensity centered at around 400 nm. The subtraction spectra are in agreement with the coloration of the samples, since the broad absorption band with uniform intensity present in the spectrum of the undoped KGdP results in the dark region (Fig. 5.a), the non-existence of such band in the spectrum of the Ce-doped sample results in a colorless sample. The broad absorption band with higher absorbance in the blue region results in the brown-yellowish region in the Pr-doped KGdP samples (Fig. 5.b). The difference in absorbance between the spectra before and after the X-ray irradiation is very low in all cases; although it should be taken into account that, the spectra obtained after the irradiation were measured after 5-7 days of recovering, so it is clear that the absorbance was higher just after irradiating the samples and this caused the coloration of the samples. The no appearance of radiation-induced absorption bands after several days of recovery and the no color change visible to the naked eye in the Ce-doped KGdP samples could indicate that these samples might not suffer from radiation damage.

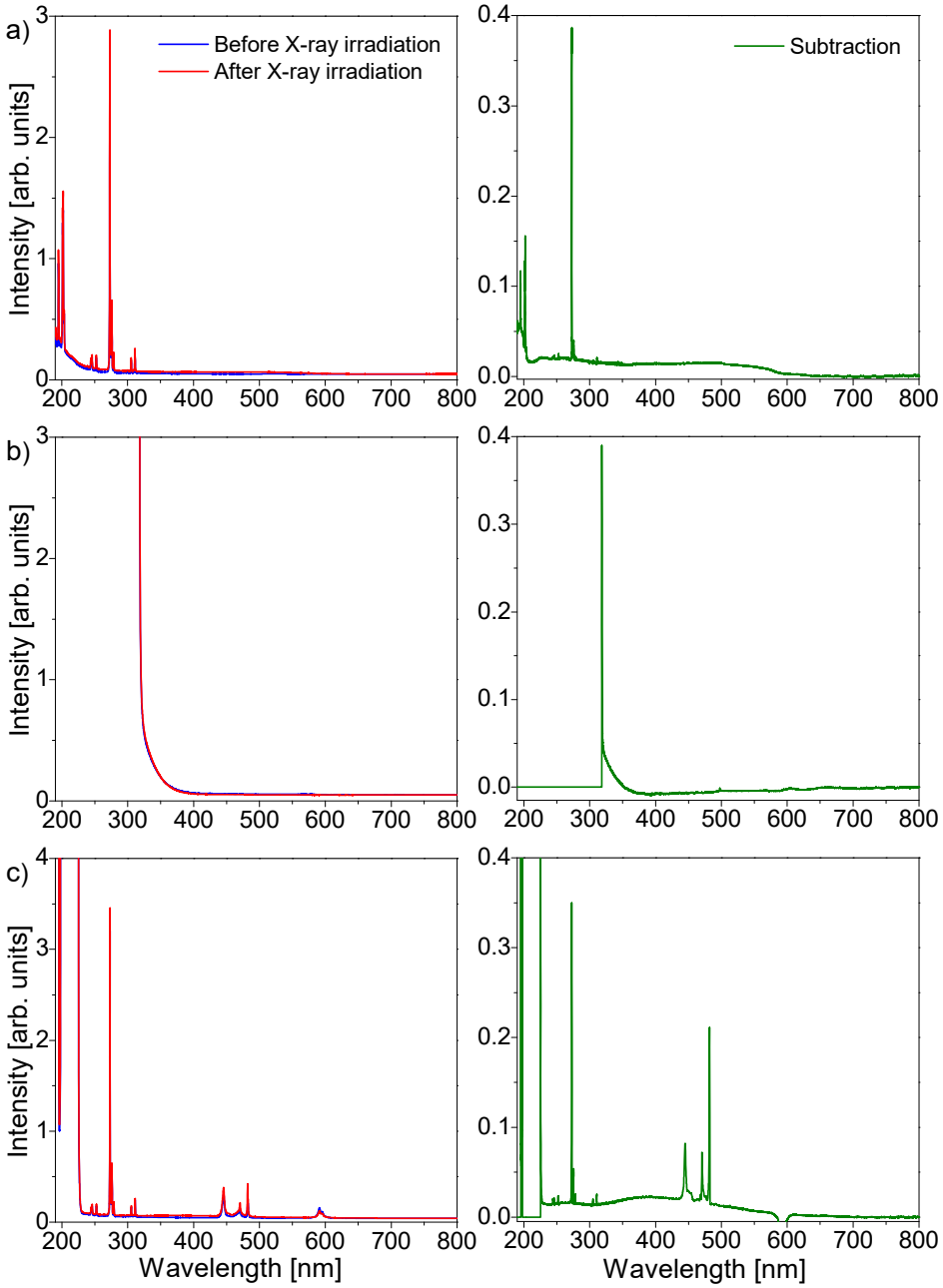

Fig. 6. Optical absorption spectra before and 5-7 days after continued X-ray irradiation (left) and the spectra resulting from the subtraction of the first data from the second one (right) for a) undoped KGdP, b) 1 at. % Ce:KGdP and c) 1 at. % Pr:KGdP single crystals.

As can be seen, the broad radiation-induced absorption band observed in the subtraction spectrum of the undoped KGdP sample is similar to that observed in the Pr-doped KGdP sample. Since this band is present in the undoped sample and only in one of the two doping ions used in this work, this behavior has been attributed to the formation of color centers related to defects in the crystal lattice, in particular due to the existence of oxygen vacancies that

probably appeared in the crystal growth process. Therefore, according to the observed change in coloration, the undoped and Pr-doped KGdP samples should have more oxygen vacancies after the crystal growth than the Ce-doped KGdP samples.

Due to the capture of electrons by oxygen vacancies and the sequential capture of charge carriers by the Ce^{3+}, Pr^{3+} and Gd^{3+} ions (see sections 3.2.2 and 3.2.4), there could be competition between these two processes and this would affect to the scintillation mechanism. In addition to this, the fact that the emission bands corresponding to the $5d_1 \rightarrow 4f$ transitions of Pr^{3+} overlap with the radiation-induced absorption band could also affect.

4. CONCLUSIONS

In the present paper, X-ray excited radioluminescence (RL) studies of type III $KGd(PO_3)_4$ bulk single crystals doped with Ce^{3+} and Pr^{3+} ions at different concentrations have been reported for the first time up to now. The RL spectra of the Ce:KGdP samples obtained after exciting them with different X-ray energies show an intense band extending from 300 to 385 nm, which has been ascribed to the $5d_1 \rightarrow {}^2F_{5/2}$ and $5d_1 \rightarrow {}^2F_{7/2}$ transitions of Ce^{3+} in KGdP, and other bands with lower intensity in the visible region that belong to $4f \rightarrow 4f$ transitions of Gd^{3+}. Since the band corresponding to the ${}^6P_{3/2,5/2,7/2} \rightarrow {}^8S_{7/2}$ transitions of Gd^{3+} (around 312 nm) is not present when KGdP is doped with Ce^{3+}, this behavior has been attributed to a very efficient energy transfer from the ${}^6P_J$ levels of Gd^{3+} to the $5d_1$ level of Ce^{3+}. In addition, bidirectional energy transfer processes between the $5d_5$ level of Ce^{3+} and the ${}^6F_J$ and ${}^6G_J$ levels of Gd^{3+} might take place. Among the concentrations studied, the doping level of Ce^{3+} in KGdP that provides the highest intensity of the emission band corresponding to the $5d_1 \rightarrow {}^2F_{5/2,7/2}$ transitions is 0.5 at. % of Ce^{3+} substituting Gd^{3+}. In contrast, the RL spectra of the Pr:KGdP samples obtained reveal the presence of the Gd^{3+} emission band centered at 312 nm belonging to the ${}^6P_{3/2,5/2,7/2} \rightarrow {}^8S_{7/2}$ transitions, this being the most intense band. These spectra also show two bands centered around 236 and 259 nm, corresponding to the $5d_1 \rightarrow {}^3H_{4,5,6}, {}^3F_2$ and $5d_1 \rightarrow {}^3F_{3,4}, {}^1G_4$ transitions of Pr^{3+} in KGdP, respectively. Additionally, other bands with lower intensity in the visible region, which have been attributed to $4f \rightarrow 4f$ transitions of Gd^{3+} or the ${}^1D_2 \rightarrow {}^3H_4$ and ${}^3P_0 \rightarrow {}^3H_6$ transitions of Pr^{3+} depending on the excitation energy have also been observed. In the Pr:KGdP samples, bidirectional energy transfer processes are also expected, in this case, between the $5d_{2,3}$ levels of Pr^{3+} and the Gd^{3+} $4f$ levels of higher energy. After exciting the samples under prolonged X-ray radiation, change in coloration in the region irradiated was observed in the undoped and Pr-doped KGdP samples, but not in the Ce-doped KGdP samples. A radiation-induced absorption band extending from 190 to 600 nm has been observed in the optical absorption spectra of the undoped and Pr-doped KGdP samples after X-ray irradiation, which could be related to the existence of color centers due to the presence of oxygen vacancies in the crystalline lattice. In future works, it would be interesting to perform decay time measurements under X-ray radiation to know the scintillation mechanism in these samples, as well as X-ray photoelectron spectroscopy (XPS) measurements of type III $KCe(PO_3)_4$ and $KPr(PO_3)_4$ single crystals in order to estimate the energy differences between the top of the valence band and the $4f$ ground state of Ce^{3+} and of Pr^{3+}, respectively.

ACKNOWLEDGMENTS

This work was supported by the Agencia Estatal de Investigación/Fondo Europeo de Desarrollo Regional (AEI/FEDER, UE) (MAT2016-75716-C2-1-R); and the Agència de Gestió d'Ajuts Universitaris i de Recerca (AGAUR) (2017 SGR 755, 2015 FI_B 00711, 2016 FI_B1 00113, 2017 FI_B2 00017). The authors thank ALBA Synchrotron for allocating beamtime at BL22-CLAESS beamline under the project with proposal number 2016091932, and Carlo Marini for his help and technical support during the radioluminescence measurements.

Disclosures

The authors declare no conflicts of interest.

REFERENCES

1. T. Yanagida, “Inorganic scintillating materials and scintillation detectors,” Proc. Jpn. Acad. Ser. B **94**, 75-97 (2018).
2. M. Khoshakhlagh, J.P. Islamian, S. M. Abedi, B. Mahmoudian, “Development of scintillators in nuclear medicine,” World J. Nucl. Med. **14**, 156-159 (2015).
3. S. Heller, P. Zanzonico, “Nuclear probes and intraoperative gamma cameras,” Semin. Nucl. Med. **41**, 166-181 (2011).
4. M. Nikl, “Scintillation detectors for x-rays,” Meas. Sci. Technol. **17**, R37-R54 (2006).
5. O. Sidletskiy, A. Belsky, A. Gektin, S. Neicheva, D. Kurtsev, V. Kononets, C. Dujardin, K. Lebbou, O. Zelenskaya, V. Tarasov, K. Belikov, B. Grinyov, “Structure−property correlations in a Ce-doped $(Lu,Gd)_2SiO_5$:Ce scintillator,” Cryst. Growth Des. **12**, 4411-4416 (2012).
6. M. Nikl, A. Yoshikawa, “Recent R&D trends in inorganic single-crystal scintillator materials for radiation detection,” Adv. Opt. Mater. **3**, 463-481 (2015).
7. F. G. A. Quarati, I. V. Khodyuk, C. W. E. van Eijk, P. Quarati, P. Dorenbos, “Study of La-138 radioactive decays using $LaBr_3$ scintillators,” Nucl. Instrum. Methods Phys. Res. Sect. A **683**, 46-52 (2012).
8. E. V. D. van Loef, P. Dorenbos, C. W. E. van Eijk, “The scintillation mechanism in $LaCl_3:Ce^{3+}$,” J. Phys.: Condens. Matter **15**, 1367-1375 (2003).
9. P. Dorenbos, E. V. D. van Loef, A. P. Vink, E. van der Kolk, C. W. E. van Eijk, K. Krämer, H. U. Güdel, W. M. Higgins, K. S. Shah, “Level location and spectroscopy of Ce^{3+}, Pr^{3+}, Er^{3+}, and Eu^{2+} in $LaBr_3$,” J. Lumin. **117**, 147-155 (2006).
10. A. M. Srivastava, J. S. Vartuli, S. J. Duclos, P. A. Schmidt, S. B. Chaney, U. Happek, “Luminescence of Pr^{3+} doped $LuCl_3$ and $LuBr_3$ under intraconfigurational (4f(2) -> 4f(1)5d(1)) and band gap excitation,” IEEE Trans. Nucl. Sci. **56**, 986-988 (2009).
11. P. Lecoq, A. Annenkov, A. Gektin, M. Korzhik, C. Pedrini, Introduction: How to answer high light yield, short decay time, and good energy resolution, in: Inorganic scintillators for detector systems: Physical principles and crystal engineering, Springer Berlin Heidelberg, The Netherlands, 2006, pp 81-82.
12. I. Adell, M. C. Pujol, R. M. Solé, M. Lancry, N. Ollier, M. Aguiló, F. Díaz, “Single crystal growth, optical absorption and luminescence properties under VUV-UV synchrotron excitation of type III Pr^{3+}:$KGd(PO_3)_4$,” Sci. Rep. (2020), accepted article.
13. T. Shalapska, G. Stryganyuk, P. Demchenko, A. Voloshinovskii, P. Dorenbos, “Luminescence properties of Ce^{3+}-doped $LiGdP_4O_{12}$ upon vacuum-ultraviolet and x-ray excitation,” J. Phys.: Condens. Matter **21**, 445901 (2009).
14. J. Zhong, H. Liang, Q. Su, J. Zhou, I. V. Khodyuk, P. Dorenbos, “Radioluminescence properties of Ce^{3+}-activated $MGd(PO_3)_4$ (M = Li, Na, K, Cs),” Opt. Mater. **32**, 378-381 (2009).
15. A. Lukowiak, L. Marciniak, I. Vasilchenko, C. Armellini, A. Chiasera, A. Vaccari, M. Ferrari, D. Dorosz, W. Strek, “Phosphate-based glasses and nanostructures,” in Proceedings of the 18th International Conference on Transparent Optical Networks (ICTON), (IEEE, 2016), We.C6.2.
16. Z. G. Mazurak, E. Lukowiak, B. Jezowska-Trzebiatowska, “Growth and spectroscopic properties of the Pr^{3+} ions in the $LiPrP_4O_{12}$ single crystals,” J. Mol. Struct. **115**, 31-35 (1984).
17. K. Horchani, J.C. Gâcon, C. Dujardin, “Scintillation properties of $CsPrP_4O_{12}$ and RbPr P_4O_{12},” Nucl. Instrum. Method. A **486**, 283-287 (2001).
18. I. Parreu, J. J. Carvajal, X. Solans, F. Díaz, M. Aguiló, “Crystal structure and optical characterization of pure and Nd-substituted type III $KGd(PO_3)_4$,” Chem. Mater. **18**, 221-228 (2006).
19. I. Parreu, R. Solé, J. Massons, F. Díaz, M. Aguiló, “Crystal growth and characterization of type III Ytterbium-doped $KGd(PO_3)_4$: A new nonlinear laser host,” Chem. Mater. **19**, 2868-2876 (2007).
20. R. Solé, X. Ruiz, M. C. Pujol, X. Mateos, J. J. Carvajal, M. Aguiló, F. Díaz, “Physical properties of self-flux and WO_3-containing solutions useful for growing type III $KGd(PO_3)_4$ single crystals,” J. Cryst. Growth **311**, 3656-3660 (2009).
21. J. A. Bearden, A. F. Burr, “Reevaluation of X-ray atomic energy levels,” Rev. Mod. Phys. **39**, 125-142 (1967).
22. P. Luger, Generation of X-rays, in: Modern X-ray analysis on single crystals, Walter de Gruyter, Berlin, Germany, 1980, pp 80.
23. C. Suryanarayana, M. Grant Norton, X-rays and diffraction, in: X-ray diffraction: A practical approach, Plenum Press, New York, NY, 1998, pp 12.
24. I. Adell, R. M. Solé, M. C. Pujol, M. Lancry, N. Ollier, M. Aguiló, F. Díaz, “Single crystal growth, optical absorption and luminescence properties under VUV-UV synchrotron excitation of type III Ce^{3+}:$KGd(PO_3)_4$, a promising scintillator material,” Sci. Rep. **8**, 11002 (2018).
25. G. H. Dieke, H. M. Crosswhite, “The spectra of the doubly and triply ionized Rare Earths,” Appl. Opt. **2**, 675-686 (1963).
26. R. T. Wegh, A. Meijerink, R. J. Lamminmaki, J. Hölsa, “Extending Dieke's diagram,” J. Lumin. **87-9**, 1002-1004 (2000).
27. R. T. Wegh, H. Donker, A. Meijerink, R. Lamminmäki, J. Hölsä, “Vacuum-ultraviolet spectroscopy and quantum cutting for Gd^{3+} in $LiYF_4$,” Phys. Rev. B **56**, 13841-13848 (1997).

28. Z. Yang, J. H. Lin, M. Z. Su, Y. Tao, W. Wang, "Photon cascade luminescence of Gd^{3+} in $GdBaB_9O_{16}$," J. Alloys Compd. **308**, 94-97 (2000).
29. C. Pédrini, D. Bouttet, C. Dujardin, A. Belsky, A. Vasil'ev, "Energy transfer and quenching processes in cerium-doped scintillators," in Proceedings of the International Conference on Inorganic Scintillators and Their Applications (SCINT), P. Dorenbos and C. W. E. van Eijk, Eds. (Delft University Press, 1995), pp 103-110.
30. P. Lecoq, A. Annenkov, A. Gektin, M. Korzhik, C. Pedrini, Scintillation mechanisms in inorganic scintillators, in: Inorganic scintillators for detector systems: Physical principles and crystal engineering, Springer Berlin Heidelberg, The Netherlands, 2006, pp 81-95.
31. C. Pédrini, "Scintillation mechanisms and limiting factors on each step of relaxation of electronic excitations," Phys. Solid State **47**, 1406-1411 (2005).
32. A. J. Wojtowicz, "Scintillation mechanism: the significance of variable valence and electron-lattice coupling in R.E.-activated scintillators," in Proceedings of the International Conference on Inorganic Scintillators and Their Applications (SCINT), P. Dorenbos and C. W. E. van Eijk, Eds. (Delft University Press, 1995), pp 95-102.
33. P. A. Rodnyi, Cerium-activated compounds, in: M. J. Weber (Ed.), Physical processes in Inorganic scintillators, CRC Press LLC, Boca Raton, FL, 1997, pp 152-154.
34. P. Lecoq, A. Annenkov, A. Gektin, M. Korzhik, C. Pedrini, Specific killer ions, in: Inorganic scintillators for detector systems: Physical principles and crystal engineering, Springer Berlin Heidelberg, The Netherlands, 2006, pp 88-89.
35. C. Dujardin, C. Pedrini, J. C. Gâcon, A. G. Petrosyan, A. N. Belsky, A. N. Vasil'ev, "Luminescence properties and scintillation mechanisms of cerium- and praseodymium-doped lutetium orthoaluminate," J. Phys.: Condens. Matter **9**, 5229-5243 (1997).
36. A. Canning, A. Chaudhry, R. Boutchko, N. Grønbech-Jensen, "First-principles study of luminescence in Ce-doped inorganic scintillators," Phys. Rev. B **83**, 125115 (2011).
37. P. Lecoq, A. Annenkov, A. Gektin, M. Korzhik, C. Pedrini, Limitation in charge carriers capture probability, in: Inorganic scintillators for detector systems: Physical principles and crystal engineering, Springer Berlin Heidelberg, The Netherlands, 2006, pp 88.
38. M. Nikl, V. Babin, J. Pejchal, V. V. Laguta, M. Buryi, J. A. Mares, K. Kamada, S. Kurosawa, A. Yoshikawa, D. Panek, T. Parkman, P. Bruza, K. Mann, M. Müller, "The stable Ce^{4+} center: A new tool to optimize Ce-doped oxide scintillators," IEEE Trans. Nucl. Sci. **63**, 433-438 (2016).
39. S. Blahuta, A. Bessiere, B. Viana, P. Dorenbos, V. Ouspenski, "Evidence and consequences of Ce^{4+} in LYSO:Ce,Ca and LYSO:Ce,Mg single crystals for medical imaging applications," IEEE Trans. Nucl. Sci. **60**, 3134-3141 (2013).
40. D. Ding, H. Feng, G. Ren, M. Nikl, L. Qin, S. Pan, F. Yang, "Air atmosphere annealing effects on LSO:Ce crystal" IEEE Trans. Nucl. Sci. **57**, 1272-1277 (2010).
41. M. Nikl, K. Kamada, V. Babin, J. Pejchal, K. Pilarova, E. Mihokova, A. Beitlerova, K. Bartosiewicz, S. Kurosawa, A. Yoshikawa, "Defect engineering in Ce-doped aluminum garnet single crystal scintillators," Cryst. Growth Des. **14**, 4827-4833 (2014).
42. P. Dorenbos, T. Shalapska, G. Stryganyuk, A. Gektin, A. Voloshinovskii, "Spectroscopy and energy level location of the trivalent lanthanides in $LiYP_4O_{12}$," J. Lumin. **131**, 633-639 (2011).
43. H. Liang, Z. Tian, H. Lin, M. Xie, G. Zhang, P. Dorenbos, Q. Su, "Photoluminescence and radioluminescence of pure and Ce^{3+} activated $Na_3Gd(PO_4)_2$," Opt. Mater. **33**, 618-622 (2011).
44. M. Kucera, M. Hanus, Z. Onderisinova, P. Prusa, A. Beitlerova, M. Nikl, "Energy transfer and scintillation properties of Ce^{3+} doped $(LuYGd)_3(AlGa)_5O_{12}$ multicomponent garnets," IEEE Trans. Nucl. Sci. **61**, 282-289 (2014).
45. M. Rathaiah, M. Kucera, J. Pejchal, A. Beitlerova, R. Kucerkova, M. Nikl, "Epitaxial growth, photoluminescence and scintillation properties of Gd^{3+} co-doped $YAlO_3:Ce^{3+}$ films," Radiat. Meas. **121**, 86-90 (2019).
46. T. Shalapska, G. Stryganyuk, P. Demchenko, A. Voloshinovskii, P. Dorenbos, "Luminescence properties of Ce^{3+}-doped $LiGdP_4O_{12}$ upon vacuum-ultraviolet and x-ray excitation," J. Phys.: Condens. Matter **21**, 445901 (2009).
47. X. Qin, X. Liu, W. Huang, M Bettinelli, X. Liu, "Lanthanide-activated phosphors based on 4f-5d optical transitions: theoretical and experimental aspects," Chem. Rev. **117**, 4488-4527 (2017).
48. Z. Yang, J. H. Lin, M. Z. Su, Y. Tao, W. Wang, "Photon Cascade Luminescence of Gd^{3+} in $GdBaB_9O_{16}$," J. Alloys Compd. **308**, 94-97 (2000).
49. Y. Wu, G. Ren, "Energy transfer and radiative recombination processes in $(Gd,Lu)_3Ga_3Al_2O_{12}:Pr^{3+}$ scintillators," Opt. Mater. **35**, 2146-2154 (2013).
50. I. Carrasco, K. Bartosiewicz, F. Piccinelli, M. Nikl, M. Bettinelli, "Structural effects and 5d→4f emission transition shifts induced by Y co-doping in Pr-doped $K_3Lu_{1-x}Y_x(PO_4)_2$," J. Lumin. **189**, 113-119 (2017).
51. M. Nikl, A. M. Begnamini, V. Jary, D. Niznansky, E. Mihokova, "Pr^{3+} luminescence center in $Lu_2Si_2O_7$ host," Phys. Status Solidi RRL **3**, 293-295 (2009).
52. J. Pejchal, M. Buryi, V. Babin, P. Prusa, A. Beitlerova, J. Barta, L. Havlak, K. Kamada, A. Yoshikawa, V. Laguta, M. Nikl, "Luminescence and scintillation properties of Mg-codoped LuAG:Pr single crystals annealed in air," J. Lumin. **181**, 277-285 (2017).
53. K. V. Ivanovskikh, A. Meijerink, F. Piccinelli, A. Speghini, E. I. Zinin, C. Ronda, M. Bettinelli, "Optical spectroscopy of $Ca_3Sc_2Si_3O_{12}$, $Ca_3Y_2Si_3O_{12}$ and $Ca_3Lu_2Si_3O_{12}$ doped with Pr^{3+}," J. Lumin. **130**, 893-901 (2010).

54. K. Kamada, M. Nikl, S. Kurosawa, Y. Shoji, J. Pejchal, Y. Ohashi, Y. Yokota, A. Yoshikawa, “Growth and scintillation properties of praseodymium doped $(Lu,Gd)_3(Ga,Al)_5O_{12}$ single crystals,” J. Lumin. **169**, 811-815 (2016).
55. R. Y. Zhu, “Radiation damage in scintillating crystals,” Nucl. Instr. Meth. Phys. Res. A **413**, 297-311 (1998).
56. S. Burachas, Yu. Saveliev, M. Ippolitov, V. Manko, V. Lomonosov, A. Vasiliev, A. Apanasenko, A. Vasiliev, A. Uzunian, G. Tamulaitis, “Physical origin of coloration and radiation hardness of lead tungstate scintillation crystals,” J. Cryst. Growth **293**, 62-67 (2006).
57. R. Y. Zhu, H. Stone, H. Newman, T. Q. Zhou, H. R. Tan, C. F. He, “A study on radiation damage in doped BGO crystals,” Nucl. Instr. Meth. Phys. Res. A **302**, 69-75 (1991).